Chinese Journal of
POLYMER SCIENCE

ARTICLE

https://doi.org/10.1007/s10118-021-2591-2
Chinese J. Polym. Sci. **2021**, *39*, 1502–1509

Supramolecular Self-assembly Behaviors of Asymmetric Diblock Copolymer Blends with Hydrogen Bonding Interactions between Shorter Blocks Modelled by Yukawa Potentials

Xu Zhang[a], Jialiang Chen[b], Lin Xu[a*], and Tianxi Liu[a,c*]

[a] *Innovation Center for Textile Science and Technology, State Key Laboratory for Modification of Chemical Fibers and Polymer Materials, College of Materials Science and Engineering, Donghua University, Shanghai 201620, China*
[b] *National Garment and Accessories Quality Supervision Testing Center (Fujian), Fujian Provincial Key Laboratory of Textiles Inspection Technology, Fujian Fiber Inspection Center, Fuzhou 350026, China*
[c] *Key Laboratory of Synthetic and Biological Colloids, Ministry of Education, School of Chemical and Material Engineering, Jiangnan University, Wuxi 214122, China*

Electronic Supplementary Information

Abstract We employed the extended self-consistent field theory to investigate the supramolecular self-assembly behaviors of asymmetric diblock copolymer blends (AB/B′C) with hydrogen bonding interactions between shorter B and B′ blocks. The hydrogen bonding interactions are described by Yukawa potentials, where the hydrogen bonding donors and acceptors were modelled as two blocks smeared with opposite screened charges. The hierarchical microstructures with parallelly packed lamellae-in-lamellae (**Lam**) and **4.8.8** Archimedean tilting pattern (**4.8.8**) were observed at lower and higher hydrogen bonding density (θ), respectively. The hierarchy of **Lam** and **4.8.8** were demonstrated by the one- and two-dimensional density profiles and the underlying order of the large-length-scale and small-length-scale microstructures were also clarified. It was found that the **4.8.8** is favorable to the stronger hydrogen bonding density or interactions. As θ increases, the microphase transition from **Lam** to **4.8.8** occurs at θ=0.34, which is mainly attributed to the optimization of the electrostatic energy and conformational entropy with sacrificing the interfacial energy. This work can provide a new strategy to understand the supramolecular self-assembly as well as the mechanism behind the formation of complex hierarchical microstructures.

Keywords Supramolecular self-assembly; Hydrogen bond; Block copolymer; Self-consistent field theory; Hierarchical microstructure

Citation: Zhang, X.; Chen. J.; Xu, L.; Liu, T. Supramolecular self-assembly behaviors of asymmetric diblock copolymer blends with hydrogen bonding interactions between shorter blocks modelled by Yukawa potentials. *Chinese J. Polym. Sci*. **2021**, *39*, 1502–1509.

INTRODUCTION

Supramolecular chemistry, first proposed by Jean-Marie Lehn in the presentation lecture for the 1987 Nobel prize in Chemistry awarded jointly to Donald J. Cram, Jean-Marie Lehn, and Charles J. Pedersen, is defined as "chemistry beyond the molecule", bearing on the organized entities of higher complexity that arises from the association of two or more chemical species combined by intermolecular forces,[1,2] so-called noncovalent or supramolecular interactions,[3] including molecular recognition,[4,5] host-guest interactions,[5–8] π-π stacking,[9–12] and hydrogen bonding,[12–15] *etc*. Rather than the classical molecular chemistry based on covalently bonding between two or more atoms, the supramolecular chemistry adopts the approach of molecular self-assembly based on supramolecular interactions to produce supramolecular architecture or assemblies varying in size, and/or composition.[10,16] Supramolecular polymer is a kind of material connecting chemically dissimilar polymers into a larger and dynamic macromolecular architecture.[16–18] Superior to the traditional way to produce polymer materials,[19–22] the supramolecular polymer would provide a greater platform for fabricating polymer materials with highly tunable properties, such as environmental adaptation[23] and self-repairing,[24] *etc*.

Inspired by the capacity of supramolecular polymers to self-assembled into complex or hierarchical microstructures with diverse functions, growing attention has been paid to design the constructing blocks as well as the corresponding supramolecular interactions to manipulate the supramolecular self-assembly behaviors.[25–31] For example, Gruschwitz *et al*.[30] demonstrated that the phase transitions from spherical to cylindrical morphologies in aqueous solutions can significantly be shifted to favor the assembly of supramolecular

* Corresponding authors, E-mail: lxu@dhu.edu.cn (L.X.)
E-mail: txliu@dhu.edu.cn,
txliu@jiangnan.edu.cn (T.L.)

Received March 22, 2021; Accepted April 14, 2021; Published online June 18, 2021

© Chinese Chemical Society
Institute of Chemistry, Chinese Academy of Sciences

polymer bottlebrushes by introducing the strong directed hydrogen bonds to an amphiphilic polymer. Thanks to the strong hydrogen bonding interactions based on the presented benzene trisureas, the supramolecular polymer bottlebrushes can self-assemble into cylinders, which overcomes the challenge of a forced self-assembly of polymers forming cylindrical structures in water as the often-required hydrophobic shielding induces forces to minimize the surface area. The straightforward synthesis and versatile design rendered the presented systems an interesting blueprint for the development of more advanced supramolecular polymer bottlebrushes and multifunctional nanostructures. Moreover, Lin *et al*.[31] have prepared a series of side-chain supramolecular polymer complexes containing proton acceptor triblock copolymer hydrogen bonded with two generations of proton donor bent-core mesogenic dendritic pendants for investigation on the hierarchical self-assembly behaviors. It was confirmed that the hierarchical lamellar domains of corresponding tetragonal and hexagonal arrangements in different generations of dendritic proton donors were self-assembled with triblock copolymer proton acceptor to induce respective BCC (body-centered cubic) and FCC (face-centered cubic) structures. The shear alignments of characteristic cylindrical column phase micro-domains were developed for the first time to control the unique hierarchical constructions of functionalized self-assembled bent-core structures by utilization of various generations of dendritic proton donors to be hydrogen-bonded with triblock copolymer proton acceptor.

In addition to the experiments, theory and simulations were always utilized to study the self-assembly behaviors of supramolecular polymers as well as the properties of polymeric systems.[32–35] Xu and co-workers have conceptually designed the multicompartment gels with supramolecular characteristics, where the mechanical properties of supramolecular multicompartment gels under uniaxial tension are studied by coupling the dissipative particle dynamics simulations with the nonequilibrium deformation technique.[36] It was discovered that the high toughness and recovery properties of the supramolecular multicompartment gels are tightly related to the structural relaxation of grafts and the association-disassociation dynamics of hydrogen bonds. The reported simulations also reveal the physical origin of the distinct mechanical properties of the supramolecular gels, which would provide useful guidance for designing functional gels with superior toughness. Self-consistent field theory (SCFT), a powerful theory method successful in discovering the self-assembly behaviors of complex polymeric systems,[37–39] has already been applied to supramolecular polymers.[17,40–43] In our previous work, we have developed a self-consistent field theory coupled with the screened Poisson equation to study the supramolecular self-assembly behaviors of symmetric diblock copolymer blends with hydrogen bonding interactions described by Yukawa potentials in a more reasonable way.[40] It was found that the appearance of observed parallel/perpendicular lamellae-in-lamellae microstructures depends on the strength of hydrogen-bonding interactions related to the density of hydrogen bonds and the characteristic lengths of the Yukawa potentials. However, in the former published work, we only examined the supramolecular self-assembly behaviors of symmetric diblock copolymer blends. The developed SCFT method could be readily further applied to more complicated supramolecular polymeric systems with hydrogen bonding interactions, such as asymmetric diblock copolymer blends.

To compensate for the limitation, we use the former extended SCFT method coupled with Yukawa potentials to illustrate the supramolecular self-assembly behaviors of asymmetric diblock copolymer blends (AB/B′C) with hydrogen bonding interactions between shorter B and B′ blocks. Similarly, the hydrogen bonding donors and acceptors are modelled as two charged blocks smeared with opposite screened charges. The effect of hydrogen bonding density on the supramolecular self-assembly behaviors was examined. Two typical hierarchical microstructures, parallelly packed lamellae-in-lamellae (**Lam**) and **4.8.8** microstructures Archimedean tilling pattern (**4.8.8**), were observed at lower and higher hydrogen bonding density, where the **4.8.8** hierarchical microstructures prefer the supramolecular asymmetric diblock copolymer blends with relatively stronger hydrogen bonding interactions. It also reveals that the formation of **4.8.8** hierarchical microstructures at stronger hydrogen bonding interactions is preferred by the optimization of electrostatic energy and the conformational entropy with the sacrifice of interfacial energy. The results obtained from the present work could provide a new strategy to comprehend the complex self-assembly behaviors of copolymers with supramolecular interactions and the mechanism behind the microphase transitions among the observed hierarchical microstructures.

METHODS AND MODEL

As shown in Fig. 1, the hydrogen bonding interactions between shorter B and B′ blocks are modelled by Yukawa potentials:

$$\psi(\mathbf{r}) = -\eta e^{-\lambda|\mathbf{r}|}/|\mathbf{r}| \quad (1)$$

where η and λ are the two characteristic lengths of the Yukawa potential. The η is the amplitude of Yukawa potential related to the dielectric permittivity and the λ is the screening length that determines the range of Yukawa potential. The hydrogen bonding interactions attached blocks (B and B′) are smeared with opposite screened charges. The valence number and corresponding charge are denoted as z_I and $z_I e$, respectively, where I = A, B, B' and C, and e is the elementary charge. The AB and B′C diblock copolymers are assumed to be monodisperse with the same statistical segment length a. The

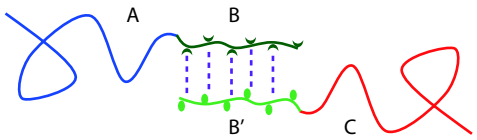

Fig. 1 Sketch of supramolecular asymmetric diblock copolymer blends (AB/B'C) with hydrogen bonding interactions between shorter B and B′ blocks. η and λ are the two characteristic lengths of the Yukawa potential $\psi(\mathbf{r})$. η is the amplitude of potential related to the dielectric permittivity and λ is the screening length that determines the range of the Yukawa potential.

https://doi.org/10.1007/s10118-021-2591-2

total statistical segments of AB and B'C are $N_{AB} = N$ and $N_{B'C} = \alpha N$, respectively. For AB (B′C) diblock copolymers, the volume fractions of A and B (B′ and C) blocks are f_A and f_B ($f_{B'}$ and f_C), respectively. Thus, $f_A + f_B = 1$ and $f_{B'} + f_C = 1$. Without exception for the simplicity of investigations, the AB and B'C diblock copolymers were treated to have the same volume-averaged fraction with equal length, *i.e.* c_{AB}=$c_{B'C}$=0.5, α=1 (or N_{AB}=$N_{B'C}$=N). The interaction strength between different blocks was set as $\chi_{AB}N$=$\chi_{AB'}N$=$\chi_{BC}N$=$\chi_{B'C}N$=20, $\chi_{AC}N$=5, and $\chi_{BB'}N$=5, where χ_{IJ} is the Flory-Huggins interaction parameter between I and J species. Then, we chose f_A=f_C=0.7, f_B=$f_{B'}$=0.3, z_A=z_C=0, z_B=−$z_{B'}$=1, θ_A=θ_C=0, θ_B=$\theta_{B'}$=θ, γ=0.01, and λ=0.1, where θ_I denotes the charge density of the I block in the supramolecular diblock copolymer blends. Therefore, the only one mutable variable in the present studies is the charge density, denoted by θ.

In the present SCFT model, the hydrogen bonding interactions are described by Yukawa potentials, which manifests that the hydrogen bonding density can be reasonably measured by the charge density (θ). In the following work, we would not make a special distinction between the charge density and hydrogen bonding and just unify the usage of hydrogen bonding density (θ) for more straightforwardly describing the nature of the hydrogen bonding interactions. The theoretical framework of the extended SCFT has been described in detail in our previous work,[40] which was omitted in the paper but completely exhibited in the electronic supplementary information (ESI, S1. Self-consistent field theory).

RESULTS AND DISCUSSION

Firstly, we examined the effect of hydrogen bonding density (θ) on the microphase behaviors of the supramolecular asymmetric diblock copolymer blends (AB/B′C) with hydrogen bonding interactions between shorter B and B′ blocks. The hierarchical microstructures self-assembled from the supramolecular blends of asymmetric diblock copolymers (AB/B′C) at various θ were observed and shown in Fig. 2, where the blue, olive, green, and red colors are assigned to A, B, B′, and C domains formed by A, B, B′, and C blocks, respectively. The two typical hierarchical microstructures, parallelly packed hierarchical lamellae-in-lamellae (denoted by **Lam**, as shown in Figs. 2a and 2a′) and hierarchical microstructures with **4.8.8** Archimedean tilling pattern (denoted by **4.8.8**, as shown in Figs. 2b and 2b′),[44] were obtained at hydrogen bonding density θ=0.20 and θ=0.50, respectively. It can be seen from Fig. 2 that the A domains (blue color) and C domains (red color) are surrounded by B domains (olive color) and B′ domains (green color), respectively, which is reasonably due to the molecular architecture restriction of the covalent bonds connected AB and B′C diblock copolymers. The intermixed BB′ domains are formed by the contacted B and B′ blocks since the attractive associations *via* hydrogen bonding interactions. In addition, the two-dimensional density profiles (Figs. 2a′ and 2b′) were further marked by the yellow dot lines (the large-length-scale microstructures) and white lines (Archimedean tilling pattern for **4.8.8**) to demonstrate the hierarchy of **4.8.8**, which emphasizes the underlying order of the large-length-scale and small-length-scale microstructures. Not surprisingly, the observed hierarchical microstructures of **Lam** and **4.8.8** self-assembled from the supramolecular block copolymer blends or star-like triblock copolymers have also been numerously observed both in experiments and simulations.[44,45] However, the hierarchical microstructures with **4.8.8** Archimedean tilling pattern self-assembled from the supramolecular asymmetric diblock copolymer blends with hydrogen bonding interactions were rarely concerned up to now, which is of great sense to understand the **4.8.8** as well as the formation mechanism behind the relationship between the hierarchical microstructures and the hydrogen bonding density, θ.

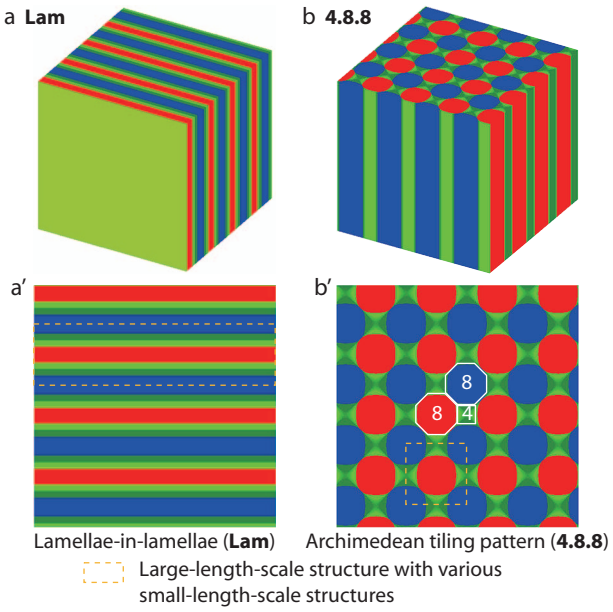

Fig. 2 (a) Parallel lamellae-in-lamellae (**Lam**) at hydrogen bonding density θ=0.20 and (b) Archimedean tilling pattern (**4.8.8**) at hydrogen bonding density θ=0.50 self-assembled from the supramolecular asymmetric diblock copolymer blends AB/B'C. The (a′) and (b′) shows the corresponding two-dimensional density profile of (a) and (b), respectively. The blue, olive, green, and red colors are assigned to A, B, B', and C blocks, respectively.

To get more deep insight into the self-assembled hierarchical microstructures, the one-dimensional density profiles of each block for **Lam** and **4.8.8** along the chosen x direction (indicated by white arrows) were analyzed, as illustrated in Figs. 3(a) and 3(b), respectively. From Fig. 3, we can see that the hydrogen bonding donors and acceptors (*i.e.*, B and B′ blocks) are separated into two microphase domains (denoted by B and B′ domains). Due to the covalently bonding restriction, the B and B′ blocks must localize at the two sides of A and C domains, respectively. As shown in Fig. 3(b) and Fig. S1 (in ESI, S2. One-dimensional density distributions), the A and C blocks are contacted with each other to form A/C interfaces, which is not particularly surprising due to the fact that the A/C contacts are energetically favored in terms of interfacial energy because of the frustrated interaction parameters: $\chi_{AC}N$=5<$\chi_{AB}N$=$\chi_{AB'}N$=$\chi_{BC}N$=$\chi_{B'C}N$=20.

For the purpose of clarifying the microphase transition from **Lam** to **4.8.8** (*i.e.*, the phase transition of **Lam**-to-**4.8.8**), we have calculated the variation of the free energies upon the formation of the obtained hierarchical microstructures of **Lam** and **4.8.8**. Fig. 4 shows the changes of free energy for **Lam** and **4.8.8** as a function of hydrogen bonding density, θ.

https://doi.org/10.1007/s10118-021-2591-2

As can be seen from Fig. 4, the **Lam** is shown to be more stable than the **4.8.8** at relatively smaller value of hydrogen bonding density (θ), indicating that the hierarchical microstructures can be transformed from **Lam** to **4.8.8** with the increasing hydrogen bonding density, θ. The phase transition of **Lam**-to-**4.8.8** is roughly at hydrogen bonding density θ=0.34, which is the intersection of the two free energy curves and also marked in Fig. 4. Because the increase in hydrogen bonding density (θ) leads to an increase in the attractive (*i.e.*, hydrogen bonding) interactions between B and B′ blocks, implying that the hierarchical microstructures with **4.8.8** Archimedean tilling pattern are preferred for the supramolecular asymmetric diblock copolymer blends with stronger hydrogen bonding interactions between shorter B and B′ blocks.

In order to further clarify the effect of hydrogen bonding strength on the hierarchical microstructures as well as the microphase transition of **Lam**-to-**4.8.8**, the domain spacings for the supramolecular asymmetric diblock copolymer blends with various hydrogen bonding density densities (θ) were also studied. Fig. 5 shows the domain spacing D/R_g of the hierarchical microstructures of **Lam** and **4.8.8** as a function of hydrogen bonding density (θ) for the supramolecular asymmetric diblock copolymer blends (AB/B′C). As can be seen, the increase in the hydrogen bonding density θ induces a slight decrease in lamellar domain spacing of both the large-length-scale ($D_{\mathbf{Lam}}$) and small-length-scale ($2D_{S\mathbf{Lam}}$) microstructures for **Lam**, which could be explained by the stronger associations between B and B′ blocks derived from the larger hydrogen bonding density. As the phase transforms from **Lam** to **4.8.8**, the domain spacing of the small-length-scale microstructures (BB′ domains) shows a slight decrease while the domain spacing size of the large-length-scale microstructures decreases significantly. Besides, the discontinuous transformation (or abrupt transition) of the domain spacing of the large-length-scale microstructures further proves that the microphase transition of **Lam**-to-**4.8.8** is the first-order phase transition. More interestingly, as the hydrogen bonding density increases beyond the phase transition point (θ=0.34), the domain spacing of the large-length-scale and small-length-scale microstructures for **4.8.8** ($D_{\mathbf{4.8.8}}$ and $D_{S\mathbf{4.8.8}}$) keeps almost unchanged. Note that the small-length-scale microstructures of **4.8.8** could provide more possible domains for forming hydrogen bonds.

Based on the above findings, we then explored the effect of hydrogen bonding density θ on the separation strength and interfacial width (denoted by w) between B and B′ blocks in the hierarchical microstructures of **Lam**, which is calculated by $\phi_B(x)-\phi_{B'}(x)$ in the BB′ domains[40] and $w=\Delta\phi_B(d\phi_B/dx)^{-1}$ at the B/B′ interface ($\Delta\phi_B$ represents the value of the largest volume fraction of B blocks in **Lam**),[46,47] respectively. Notably, the separation strength $|\phi_B(x)-\phi_{B'}(x)|$=0 and 1 (or −1) represents that the B and B′ blocks are disordered and completely separated, respectively. As can be seen from Fig. 6(a), the separation strength $\phi_B(x)-\phi_{B'}(x)$ shows a shift much closer to θ=0 as θ increases from 0.05 to 0.30, indicating that the larger hydrogen bonding density leads to weaker separation between B and B′ blocks because of the

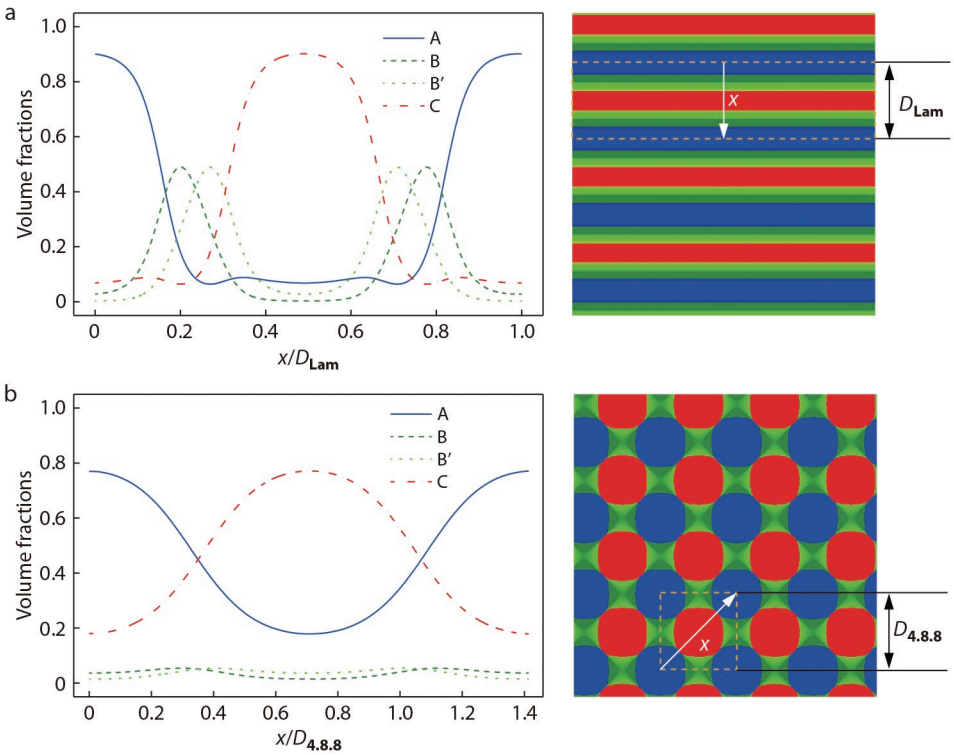

Fig. 3 One-dimensional density distributions of the blocks along the chosen x direction of (a) **Lam** at θ=0.25 and (b) **4.8.8** at θ=0.50 self-assembled from supramolecular asymmetric diblock copolymer blends AB/B′C. The D is the domain spacing size of the largen-length-scale microstructures, including **Lam** and **4.8.8**, which is indicated in the right morphological illustrations.

https://doi.org/10.1007/s10118-021-2591-2

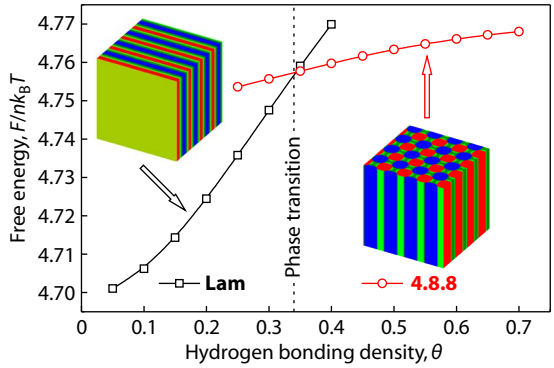

Fig. 4 Free energies as a function of hydrogen bonding density θ for the obtained **Lam** and **4.8.8** hierarchical microstructures. The intersection of the two lines is the phase transition point between **Lam** and **4.8.8** at hydrogen bonding density θ=0.34. The left and right inserts show the morphological microstructures of **Lam** and **4.8.8**, respectively.

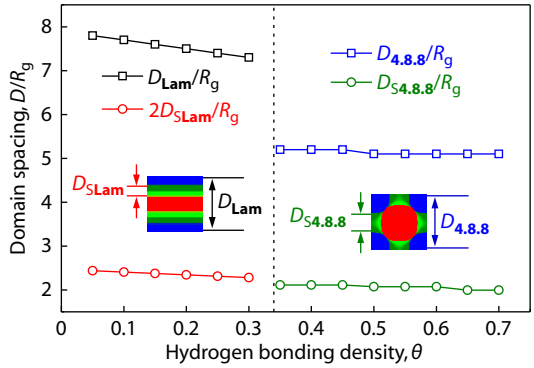

Fig. 5 Domain spacing D/R_g of **Lam** and **4.8.8** hierarchical microstructures as a function of hydrogen bonding density θ. The domain spacing size of the large-length-scale microstructures (D_{Lam} for **Lam** and $D_{4.8.8}$ for **4.8.8**) and small-length-scale microstructures ($2D_{SLam}$ for **Lam** and $D_{S4.8.8}$ for **4.8.8**) are schematically presented in the left and right inset, where only the small-length-scale microstructures of BB' domains are concerned to indicate the spacing effect on the microphase transition of **Lam**-to-**4.8.8**. The vertical short-dash line corresponds to the microphase transition of **Lam**-to-**4.8.8** at hydrogen bonding density θ=0.34.

stronger association of B and B′ blocks through hydrogen bonding interactions. This could be also reflected by the variation of the interfacial width, w, as provided in Fig. 6(b). It can be seen that the B/B′ interfaces become broader as the hydrogen bonding density θ increases from 0.05 to 0.30, similarly suggesting that the microphase separation between B and B′ blocks is weaker at relatively larger hydrogen bonding density corresponding to the stronger hydrogen bonding interactions in the supramolecular asymmetric diblock copolymer blends.

To further elaborate the effect of hydrogen bonding density, corresponding to the hydrogen bonding interaction strength, on the hierarchical microstructures (**Lam** and **4.8.8**) as well as the microphase transition of **Lam**-to-**4.8.8**, the interfacial energy (U_X/nk_BT), electrostatic energy (U_e/nk_BT), and entropic loss ($-S/nk_B$) for the supramolecular diblock copolymer blends as a function of hydrogen bonding density (θ) was

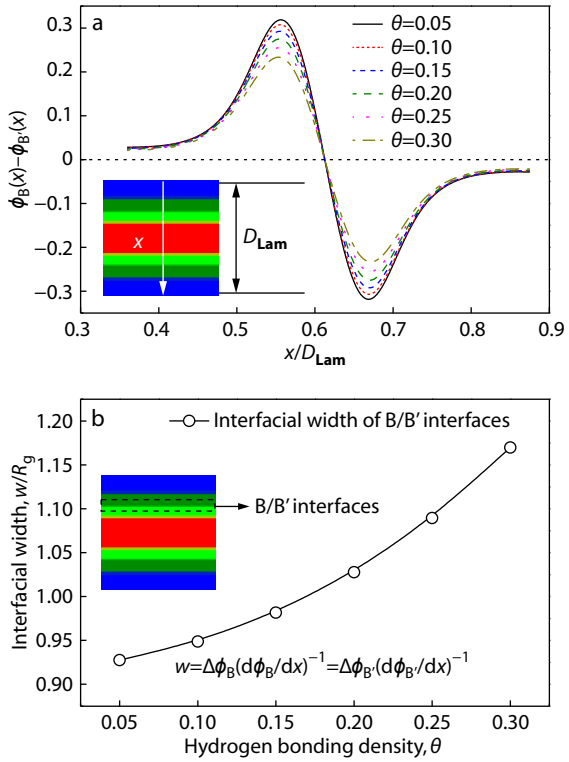

Fig. 6 (a) Separation strength calculated by $\phi_B(x)$-$\phi_{B'}(x)$ along the chosen x direction of **Lam** with various hydrogen bonding densities θ, where D_{Lam} is the lamellar domain spacing size of **Lam** as illustrated in the upper inset. (b) Interfacial width w/R_g of B/B′ interfaces (as shown in the lower inset) calculated by $\Delta\phi_B(d\phi_B/dx)^{-1}$ or $\Delta\phi_{B'}(d\phi_{B'}/dx)^{-1}$.[46,47] The horizontal short-dash line in (a) corresponds to the unseparated strength at $\phi_B(x)-\phi_{B'}(x)=0$.

analyzed and presented in Figs. 7(a)–7(c), respectively. As the hydrogen bonding density θ increases, *i.e.*, as the hydrogen bonding interaction strengthens, the interfacial energy (U_X/nk_BT) increases, whereas the electrostatic energy (U_e/nk_BT) and entropy loss ($-S/nk_B$) decreases prominently. It can be concluded that the increase of hydrogen bonding interactions is also beneficial to lower the electrostatic energy (U_e/nk_BT) and entropic loss ($-S/nk_B$) in **Lam** which makes mainly contributions to stabilize the **Lam** at relatively stronger hydrogen bonding interactions under the microphase transition point (θ<0.34). When the hydrogen bonding density θ exceeds to the phase transition point of **Lam**-to-**4.8.8** at hydrogen bonding density θ=0.34, the interfacial energy (U_X/nk_BT, Fig. 7a) shows an abrupt increase, while the electrostatic energy (U_e/nk_BT, Fig. 7b) and entropic loss ($-S/nk_B$, Fig. 7c) simultaneously jumps down sharply to a lower value. In general, the microphase transition from **Lam** to **4.8.8** is advantageous for the electrostatic energy (U_e/nk_BT) and entropic loss ($-S/nk_B$) but unfavorable for the interfacial energy (U_X/nk_BT).

According to the above results and discussion, we provided a scheme to illustrate the process of the microphase transition from **Lam** to **4.8.8**, as illustrated in Fig. 8, in which the possible conformation of polymer chains of AB and B′C asymmetric diblock copolymers in different microstructures (**Lam** and **4.8.8**) are sketched and mapped out. By combining the

https://doi.org/10.1007/s10118-021-2591-2

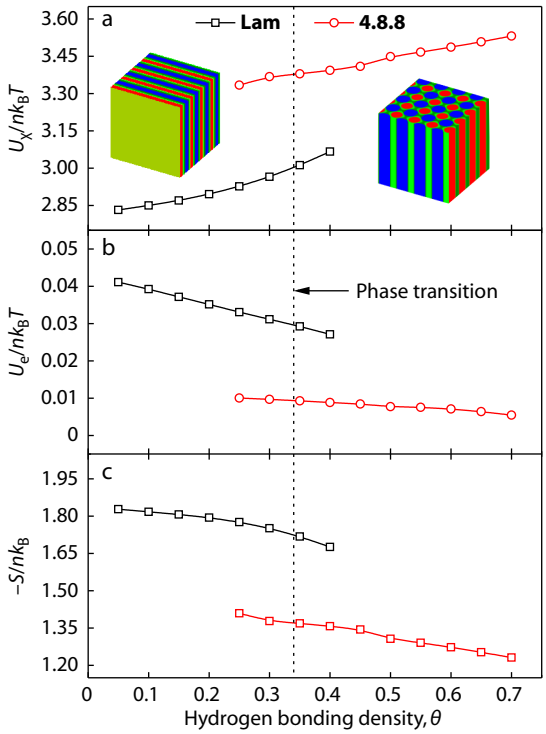

Fig. 7 (a) Interfacial energy (U_X/nk_BT), (b) electrostatic energy (U_e/nk_BT), and (c) entropic loss ($-S/nk_B$) as a function of hydrogen bonding density, θ. The left and right inset shows the morphological microstructures of **Lam** and **4.8.8**, respectively. The vertical short-dash line corresponds to the phase transition of **Lam**-to-**4.8.8** at hydrogen bonding density θ=0.34.

calculation of the domain spacing (Fig. 5), separation strength (Fig. 6a), interfacial width (Fig. 6b), interfacial energy (U_X/nk_BT, Fig. 7a), electrostatic energy (U_e/nk_BT, Fig. 7b), and entropic loss ($-S/nk_B$, Fig. 7c), the microphase transition phenomenon that the **Lam** changes to **4.8.8** increasing in the hydrogen bonding interactions could be finally explained as follows. At lower hydrogen bonding interactions, the supramolecular asymmetric diblock copolymer blends (AB/B′C) favor the parallelly packed hierarchical lamellae-in-lamellae microstructures (**Lam**) having the large domain spacing both in large-length-scale and small-length-scale microstructures (Fig. 5), where the hydrogen bonding associations between B and B′ blocks prevent the macroscopic phase separation between AB and B′C diblock copolymers. In the parallelly packed lamellar microstructures (*i.e.* **Lam**), the interfacial energy (U_X/nk_BT, in Fig. 7a) is optimized because the interfaces between immiscible blocks (A/B′, A/C, and B/C interfaces) could be maximally prohibited. However, the shorter B and B′ blocks must be strongly stretched in the small-length-scale microstructures (Figs. 8a and 8b) to form lamellar microstructures (*i.e.* BB′ lamellar domains) with comparable domain spacing to the large-length-scale lamellar microstructures (A and C lamellar domains), which significantly sacrifices the conformational entropy (Fig. 7c). With the increasing hydrogen bonding interactions (hydrogen bonding density, θ), the electrostatic energy prefers the attractive associations of B and B′ blocks through hydrogen bonding interactions (Figs. 8a to 8b), which weakens the separation between B and B′ blocks (*i.e.* decreases the separation strength and increases the interfacial width, as shown in Figs. 6(a) and 6(b), respectively) and narrows the lamellar domain spacing ($D_{\mathbf{Lam}}$ and $D_{S\mathbf{Lam}}$, Fig. 5a). The specific area of B/B′ interfaces acting as the possible domains for forming the hydrogen bonds increases (Figs. 8a to 8b) and the interfacial energy also shift upwards to larger values (Fig. 7a). Thus, this is a process to make a profit out of the electrostatic attraction and conformational entropy but to lose the interfacial energy.

As the hydrogen bonding density θ increases to the micro-

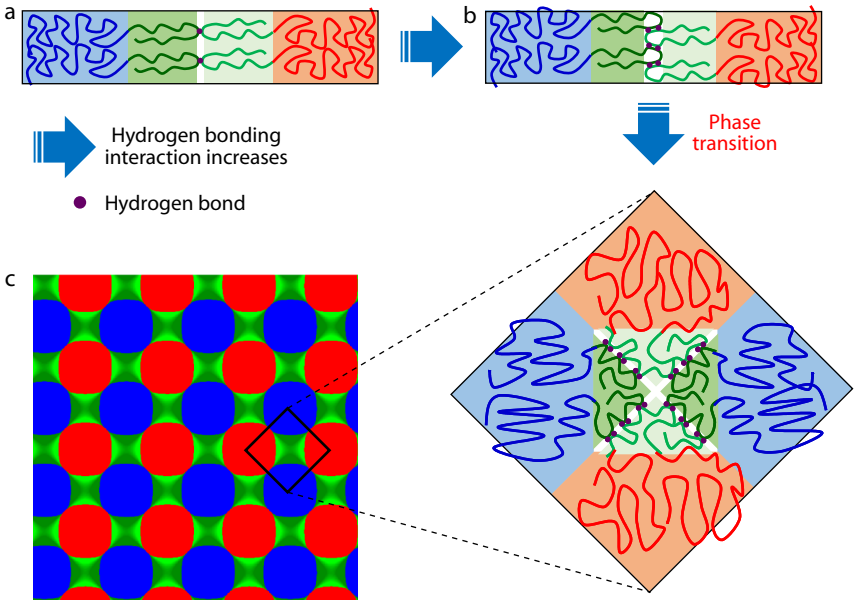

Fig. 8 Sketch of the possible conformation of AB/B′C supramolecular asymmetric diblock copolymer blends in the small-length-scale microstructures of BB′ domains, where the white domains represent the possible regions for associating B and B′ blocks and forming hydrogen bonds.

https://doi.org/10.1007/s10118-021-2591-2

phase transition point (θ=0.34), the total free energy cannot be minimized in **Lam** due to the fact that the contributions of electrostatic energy (U_e/nk_BT) and conformational entropy (or entropic loss, $-S/nk_B$) are not able to compensate for the serious sacrifice of interfacial energy, and then the hierarchical microstructures with **4.4.8** Archimedean tilling pattern are energetically favorable. Compared with **Lam**, the **4.4.8** hierarchical microstructures provide more B/B′ interfaces for forming hydrogen bonds as indicated by the white regions in Fig. 8(c). What is noteworthy is that the hydrogen bonds are associated at the B/B′ interfaces parallel to the large-length-scale lamellae (A and C domains) in the **Lam** (marked by the while regions in Figs. 8a and 8b), while there are two crossed B/B′ interfaces in the **4.8.8** (marked by the while regions in Fig. 8c). As a result, the electrostatic energy and entropic loss plunges and earns profit (Figs. 7b and 7c). However, the additional A/C interfaces comes into being in the **4.4.8**, resulting in a sudden rise in the interfacial energy (Fig. 8a). Moreover, for the **4.4.8** hierarchical microstructures, the domain spacing of the small-length-scale microstructures is relatively larger and the distribution of B/B′ interfaces is more dispersal (Fig. 8c), which is of great help to the chain conformation (Fig. 7c) and the formation of hydrogen bonds due to the larger area of B/B′ interfaces (Fig. 8c). Overall, the microphase transition from **Lam** to **4.8.8** is mainly attributed to the optimization of the electrostatic energy and conformational entropy through sacrificing the interfacial energy.

CONCLUSIONS

The extended self-consistent field theory was used to study the supramolecular self-assembly of asymmetric diblock copolymer blends (AB/B′C) with hydrogen bonding interactions between shorter B and B′ blocks, where the hydrogen bonding interactions were described by Yukawa potentials. The hydrogen bonding donors and acceptors were modelled as B and B′ blocks smeared with opposite screened charges. The hierarchical microstructures with parallelly packed lamellae-in-lamellae (**Lam**) and **4.8.8** microstructures Archimedean tilling pattern (**4.8.8**) were observed at lower and higher hydrogen bonding density. The **4.8.8** were found to be stable for the supramolecular asymmetric diblock copolymer blends with stronger hydrogen bonding interactions corresponding to the higher hydrogen bonding density (*i.e.* charge density for Yukawa potential). The results and discussion reveal that the formation of hierarchical microstructures with **4.8.8** Archimedean tilling pattern for the supramolecular asymmetric diblock copolymer at stronger hydrogen bonding interactions is favorable to the electrostatic energy and the conformational entropy by sacrificing the interfacial energy. The obtained results can provide a new strategy to tailor the complex microphase behaviors of the supramolecular polymers as well as achieve the reasonable explanation for the microphase transitions among the observed hierarchical microstructures.

Electronic Supplementary Information

Electronic supplementary information (ESI) is available free of charge in the online version of this article at http://doi.org/10.1007/s10118-021-2591-2.

ACKNOWLEDGMENTS

This work was financially supported by the Natural Science Foundation of Shanghai (No. 21ZR1402800), the Fundamental Research Funds for the Central Universities (No. 2232020D-11), the China Postdoctoral Science Foundation (No. 2021M690597) and the Open Project Program of Fujian Provincial Key Laboratory of Textiles Inspection Technology (Fujian Fiber Inspection Center) (Nos. 2020-MXJ-04).

REFERENCES

1 Lehn, J. M. Supramolecular chemistry-scope and perspectives molecules, supermolecules, and molecular devices (Nobel Lecture). *Angew. Chem. Int. Ed.* **1988**, *27*, 89–112.
2 Cheng, M. J.; Zhang, Q.; Shi, F. Macroscopic Supramolecular assembly and its applications. *Chinese J. Polym. Sci.* **2018**, *36*, 306–321.
3 Aida, T.; Meijer, E.; Stupp, S. I. Functional supramolecular polymers. *Science* **2012**, *335*, 813–817.
4 Zhao, R.; Zhou, Y. J.; Jie, K. C.; Yang, J.; Perrier, S.; Huang, F. H. Fluorescent supramolecular polymersomes based on pillararene/paraquat molecular recognition for pH-controlled drug release. *Chinese J. Polym. Sci.* **2020**, *38*, 1–8.
5 Dong, S. Y.; Zheng, B.; Wang, F.; Huang, F. H. Supramolecular polymers constructed from macrocycle-based host-guest molecular recognition motifs. *Acc. Chem. Res.* **2014**, *47*, 1982–1994.
6 Liu, C.; Li, J.; Jin, Z.; Hou, P.; Zhao, H.; Wang, L. Synthesis of graphene-epoxy nanocomposites with the capability to self-heal underwater for materials protection. *Compos. Commun.* **2019**, *15*, 155–161.
7 Ji, X.; Wang, P.; Wang H.; Huang, F. A fluorescent supramolecular crosslinked polymer gel formed by crown ether based host-guest interactions and aggregation induced emission. *Chinese J. Polym. Sci.* **2015**, *33*, 890–898.
8 Chen, J.; Hou, Y.; Li, S.; Huang, Y.; Lv, S. Host-guest complexes of β-cyclodextrin with methyl orange/methylene blue-derived multi-heteroatom doped carbon materials for supercapacitors. *Compos. Commun.* **2019**, *16*, 117–123.
9 Stupp, S. I.; Palmer, L. C. Supramolecular chemistry and self-assembly in organic materials design. *Chem. Mater.* **2014**, *26*, 507–518.
10 Gogoi, N.; Bashir, B.; Yang, Z.; Ma, P. Supramolecular assembly of leaf-like fluorescent tetraphenylethylene through polymer-directed inter-locking. *Compos. Commun.* **2019**, *11*, 45–51.
11 Xu, L.; Zhang, H. H.; Lu, Y. Y.; An, L. J.; Shi, T. F. The effects of solvent polarity on the crystallization behavior of thin π-conjugated polymer film in solvent mixtures investigated by grazing incident X-ray diffraction. *Polymer* **2020**, *190*, 122259.
12 Zhang, K.; Chen, Z.; Guo, B.; Cai, K.; Liang, Y.; Li, J.; Jin, L. Y. Self-assembly of amphiphilic linear diblock rod-coil molecules by hydrogen bond and π-π stacking interactions. *Chinese J. Polym. Sci.* **2016**, *34*, 307–315.
13 Li, J.; Zhang, P.; Chen, L.; Li, G.; Chen, H.; Jian C.; Wu, P.; Chen, M.; Zhao, X.; Song, P. Strong, tough and healable elastomer nanocomposites enabled by a hydrogen-bonded supramolecular network. *Compos. Commun.* **2020**, *22*, 100530.
14 Fan, J.; Xu, X.; Yu, W.; Wei, Z.; Zhang, D. Hydrogen-bond-driven supramolecular self-assembly of diacetylene derivatives for

topochemical polymerization in solution. *Polym. Chem.* **2020**, *11*, 1947–1954.
15 Chai, Z.; Xie, Z.; Zhang, P.; Ouyang, X.; Li, R.; Gao, S.; Wei, H.; Liu, L.; Shuai, Z. High impact resistance epoxy resins by incorporation of quadruply hydrogen bonded supramolecular polymers. *Chinese J. Polym. Sci.* **2016**, *34*, 850–857.
16 Hou, Y.; He, Z.; Wang, C.; Zhang, L.; Xuan, Q.; Wei, S.; Wang, Y.; Pan, D.; Dong B.; Wei R.; Naik, N. The recent progress of synergistic supramolecular polymers: preparation, properties and applications. *Chem. Commun.* **2021**, *57*, 1413–1429.
17 Zhang, X.; Wang, L. Q; Lin, J. P. Phase behaviors of supramolecular graft copolymers with reversible bonding. *J. Chem. Phys.* **2013**, *139*, 184901.
18 Golkaram, M.; Loos, K. A critical approach to polymer dynamics in supramolecular polymers. *Macromolecules* **2019**, *52*, 9427–9444.
19 Xu, L.; Shi, T. F.; An, L. J.; Lu, Y. Y.; Wang, L. N. Effect of interfacial adsorption on the stability of thin polymer films in a solvent-induced process. *Chinese J. Polym. Sci.* **2021**, *39*, 501–511.
20 Zhou, G. Y.; An, X. Y.; Zhou, C. Y.; Wu, Y.; Miao Y. E.; Liu, T. X. Highly porous electroactive polyimide-based nanofibrous composite anode for all-organic aqueous ammonium dual-ion batteries. *Compos. Commun.* **2020**, *22*, 100519.
21 Wang, L. N.; Zhang, H. H.; Xu, L.; Liu, B. Y.; Shi, T. F.; Jiang, S. C.; An, L. J. Dewetting kinetics of thin polymer films with different architectures: effect of polymer adsorption. *Chinese J. Polym. Sci.* **2018**, *36*, 984–990.
22 Kong, L.; Zhu, Y.; Huang, G.; Wu, J. Carbon nanodots as dual role of crosslinking and reinforcing chloroprene rubber. *Compos. Commun.* **2020**, *22*, 100441.
23 Zhou, X. H.; Li, C.; Zhu, L. F.; Zhou, X. C. Engineering hydrogels by soaking: from mechanical strengthening to environmental adaptation. *Chem. Commun.* **2020**, *56*, 13731–13747.
24 Zhang, L.; Wang, D.; Xu, L. Q.; Zhang, A. M. A supramolecular polymer with ultra-stretchable, notch-insensitive, rapid self-healing and adhesive properties. *Polym. Chem.* **2021**, *12*, 660–669.
25 Zuccaccia, D.; Pinalli, R.; De Zorzi, R.; Semeraro, M.; Credi, A.; Zuccacia, C.; Macchioni, A.; Geremia, S.; Dalcanale, E. Hierarchical self-assembly and controlled disassembly of a cavitand-based host-guest supramolecular polymer. *Polym. Chem.* **2021**, *12*, 389–401.
26 Wu, D. J.; Vonk, N. H.; Lamers, B. A. G.; Castilho, M.; Malda, J. Hoefnagels, J. P. M.; Dankers, P. Y. W. Anisotropic hygro-expansion in hydrogel fibers owing to uniting 3D electrowriting and supramolecular polymer assembly. *Eur. Polym. J.* **2020**, *141*, 110099.
27 Ye, S. H.; Wang, B.; Shi, Y. T.; Wang, B. Z.; Zhang, Y. R.; Feng, Y. Z.; Han, W. J.; Liu, C. T.; Shen, C. Y. Superhydrophobic and superelastic thermoplastic polyurethane/multiwalled carbon nanotubes porous monolith for durable oil/water separation. *Compos. Commun.* **2020**, *21*, 100378.
28 Lu, Y. Q.; Lin, J. P.; Wang, L. Q.; Zhang, L. S.; Cai, C. H. Self-assembly of copolymer micelles: higher-level assembly for constructing hierarchical structure. *Chem. Rev.* **2020**, *120*, 4111–4140.
29 Gao, L.; Gao, H. B.; Lin, J. P.; Wang, L. Q.; Wang, X. S.; Yang, C. M.; Lin, S. L. Growth and termination of cylindrical micelles *via* liquid-crystallization-driven self-assembly. *Macromolecules* **2020**, *53*, 8992–8999.
30 Gruschwitz, F. V.; Fu, M. C.; Klein, T.; Takahashi, R.; Higashihara, T.; Hoeppener, S.; Nischang, I.; Sakurai, K.; Brendel, J. C. Unraveling decisive structural parameters for the self-assembly of supramolecular polymer bottlebrushes based on benzene trisureas. *Macromolecules* **2020**, *53*, 7552–7560.
31 Lin, C. M.; Dwivedi, A. K.; Chuang, W. T.; Lin, H. C. Hierarchical self-assembly of supramolecular polymer complexes mediated by various generations of bent-core mesogenic dendrimers hydrogen-bonded with triblock copolymer. *Polymer* **2020**, *208*, 122880.
32 Payandehpeyman, J.; Mazaheri, M.; Khamehchi, M. Prediction of electrical conductivity of polymer-graphene nanocomposites by developing an analytical model considering interphase, tunneling and geometry effects. *Compos. Commun.* **2020**, *21*, 100364.
33 Monticeli, F. M.; Daou, D.; Peković, O.; Simonović, A.; Voorwald, H. J. C.; Cioffi, M. O. H. FEA simulation and experimental validation of mode I and II delamination at the carbon/glass/epoxy hybrid interface: physical-based interpretation. *Compos. Commun.* **2020**, *22*, 100532.
34 Liu, Z. J.; Xu, Z. W.; Wang, L. Q.; Lin, J. P. Distinctive optical properties of hierarchically ordered nanostructures self-assembled from multiblock copolymer/nanoparticle mixtures. *Macromol. Rapid Commun.* **2020**, *41*, 2000131.
35 Li, Q.; Wang, L. Q.; Lin, J. P.; Xu, Z. W. Distinctive morphology modifiers for polymer blends: roles of asymmetric Janus nanoparticles during phase separation. *J. Phys. Chem. B* **2020**, *124*, 4619–4630.
36 Xu, P. X.; Lin, J. P.; Zhang, L. S. Supramolecular multicompartment gels formed by ABC graft copolymers: high toughness and recovery properties. *Phys. Chem. Chem. Phys.* **2018**, *20*, 15995–16004.
37 Dong, Q.; Li, W. H. Effect of molecular asymmetry on the formation of asymmetric nanostructures in ABC-type block copolymers. *Macromolecules* **2021**, *54*, 203–213.
38 Gu, X. Y.; Li, W. H. Impact of thin-film confinement on the packing of low-coordinate spheres in bulk. *Macromolecules* **2020**, *53*, 9131–9141.
39 Li, C. C.; Dong, Q. S.; Li, W. H. Largely tunable asymmetry of phase diagrams of $A(AB)_n$ miktoarm star copolymer. *Macromolecules* **2020**, *53*, 10907–10917.
40 Zhang, X.; Lin, J. Y.; Wang, L. Q.; Zhang, L. S.; Lin, J. P.; Gao, L. Supramolecular assembly of diblock copolymer blends with hydrogen-bonding interactions modeled by Yukawa potentials. *Polymer* **2015**, *18*, 69–80.
41 Dehghan, A.; Shi, A. C. Modeling hydrogen bonding in diblock copolymer/homopolymer blends. *Macromolecules* **2013**, *46*, 5796–5805.
42 Feng, E. H.; Lee, W. B.; Fredrickson, G. H. Supramolecular diblock copolymers: a field-theoretic model and mean-field solution. *Macromolecules* **2007**, *40*, 693–702.
43 Lee, W. B.; Elliott, R.; Katsov, K.; Fredrickson, G. H. Phase morphologies in reversibly bonding supramolecular triblock copolymer blends. *Macromolecules* **2007**, *40*, 8445–8454.
44 Matsushita, Y. Creation of hierarchically ordered nanophase structures in block polymer blends various competing interactions. *Macromolecules* **2007**, *40*, 771–776.
45 Li, W. H.; Xu, Y. C.; Zhang, G. J.; Qiu, F.; Yang, Y. L.; Shi, A. C. Real-space self-consistent mean-field theory study of ABC star triblock copolymers. *J. Chem. Phys.* **2010**, *133*, 064904.
46 Matsen, M. W.; Thompson, R. B. Equilibrium behavior of symmetric ABA triblock copolymer melts. *J. Chem. Phys.* **1999**, *111*, 7139–7146.
47 Patterson, A. L.; Yu, B.; Danielsen, S. P. O.; Davidson, E. C.; Fredrickson, G. H.; Segalman, R. A. Monomer sequence effects on interfacial width and mixing in self-assembled diblock copolymers. *Macromolecules* **2020**, *53*, 3262–3272.

https://doi.org/10.1007/s10118-021-2591-2